Individual heme a and heme a3 contributions to the Soret absorption spectrum of the reduced bovine cytochrome c oxidase

Artem Diuba, Tatiana Vygodina, Natalia Azarkina, Alexander Arutyunyan, Tewfik Soulimane, Marten Vos, Alexander Konstantinov

Individual heme *a* and heme a_3 contributions to the Soret absorption spectrum of the reduced bovine cytochrome *c* oxidase

Artem V. Diuba[a1*], Tatiana V. Vygodina[b], Natalia V. Azarkina[c], Alexander M. Arutyunyan[d], Tewfik Soulimane[e], Marten H. Vos[f], Alexander A. Konstantinov[g†]

[a] Belozersky Institute of Physico-Chemical Biology, Lomonosov Moscow State University, Leninskie Gory 1, Bld.40, Moscow, Russia 119992 dyubon@gmail.com

[b] Belozersky Institute of Physico-Chemical Biology, Lomonosov Moscow State University, Leninskie Gory 1, Bld.40, Moscow, Russia 119992 vygodina@belozersky.msu.ru

[c] Belozersky Institute of Physico-Chemical Biology, Lomonosov Moscow State University, Leninskie Gory 1, Bld.40, Moscow, Russia 119992 azarkina@yahoo.com

[d] Belozersky Institute of Physico-Chemical Biology, Lomonosov Moscow State University, Leninskie Gory 1, Bld.40, Moscow, Russia 119992 alarut@genebee.msu.ru

[e] Materials and Surface Science Institute, University of Limerick, Ireland V94 T9PX Tewfik.Soulimane@ul.ie

[f] LOB, CNRS, INSERM, Ecole Polytechnique, Institut Polytechnique de Paris, Palaiseau, France 91128 marten.vos@polytechnique.edu

[g] Belozersky Institute of Physico-Chemical Biology, Lomonosov Moscow State University, Leninskie Gory 1, Bld.40, Moscow, Russia 119992

*Corresponding author; e-mail: dyubon@gmail.com

[1]Present address: Institute for Neurosciences of Montpellier, University of Montpellier, Institut National de la Santé et de la Recherche Médicale, 34091 Montpellier, France

[†]Deceased, May 1, 2020

CRediT author statement

Artem V. Diuba: Conceptualization, Methodology, Software, Validation, Formal analysis, Investigation, Resources, Data Curation, Writing - Original Draft, Writing - Review & Editing, Visualization, Project administration. **Tatiana V. Vygodina:** Methodology, Validation, Investigation, Resources, Writing - Review & Editing. **Natalia V. Azarkina**: Methodology, Validation, Investigation, Resources, Writing - Review & Editing. **Alexander M. Arutyunyan:** Methodology, Resources, Validation, Writing - Review & Editing. **Tewfik Soulimane:** Validation, Resources, Writing - Review & Editing. **Marten H. Vos:** Conceptualization,

Methodology, Validation, Formal analysis, Investigation, Resources, Data Curation, Writing - Review & Editing. **Alexander A. Konstantinov:** Conceptualization, Methodology, Validation, Writing - Original Draft, Writing - Review & Editing, Supervision, Project administration, Funding acquisition.

The authors declare that they have no known competing financial interests or personal relationships that could have appeared to influence the work reported in this paper.

Graphical abstract:

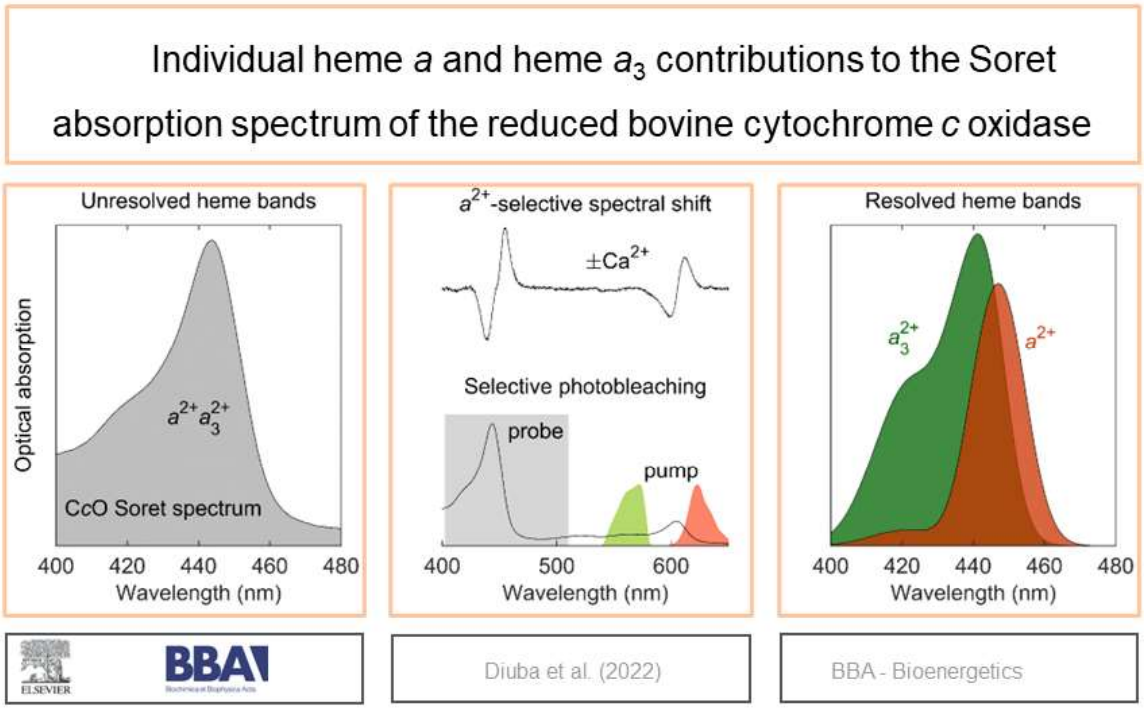

Abstract

Bovine cytochrome *c* oxidase (C*c*O) contains two hemes, *a* and a_3, chemically identical but differing in coordination and spin state. The Soret absorption band of reduced aa_3-type cytochrome *c* oxidase consists of overlapping bands of the hemes a^{2+} and a_3^{2+}. It shows a peak at ~444 nm and a distinct shoulder at ~425 nm. However, attribution of individual spectral lineshapes to hemes a^{2+} and a_3^{2+} in the Soret is controversial. In the present work, we characterized spectral contributions of hemes a^{2+} and a_3^{2+} using two approaches. First, we reconstructed bovine C*c*O heme a^{2+} spectrum using a selective Ca^{2+}-induced spectral shift of the heme a^{2+}. Second, we investigated photobleaching of the reduced *Thermus thermophilus* ba_3- and bovine aa_3-oxidases in the Soret induced by femtosecond laser pulses in the Q-band. The resolved spectra show splitting of the electronic B_{0x} -, B_{0y}-transitions of both reduced hemes. The heme a^{2+} spectrum is shifted to the red relative to heme a_3^{2+} spectrum. The ~425 nm shoulder is mostly attributed to heme a_3^{2+}.

Keywords: Cytochrome *c* oxidase, absorption spectra, femtosecond pump-probe spectroscopy.

Abbreviations:

C*c*O, cytochrome c oxidase

FWHH, full width at half-height

MCD, magnetic circular dichroism

SMR, succinate: menaquinone reductase

Highlights:

- Bovine C*c*O a^{2+} Soret band is a split electronic 447.5-nm peak with a minimal short-wavelength satellite
- a^{2+} α-band is also split
- a_3^{2+} Soret band is a split electronic 441-nm peak with a short-wavelength satellite
- Ratio of integrals under a^{2+} and a_3^{2+} Soret bands is approximately 1 to 2

1. Introduction

In mitochondrial and some bacterial respiratory chains, aa_3-type cytochrome *c* oxidase (C*c*O) catalyzes oxidation of ferrous cytochrome *c* by oxygen, converting redox potential energy to the transmembrane difference of proton electrochemical potentials, $\Delta\mu H^+$. The exergonic electron transfer coupled to proton translocation across the membrane [1] via proton channels [2–6] is mediated by two A-type hemes, low-spin 6-coordinate *a* and high-spin 5-coordinate a_3, and two copper centers: binuclear Cu_A and mononuclear Cu_B [5,7–9].

Absorption spectra of hemes *a* and a_3, sensitive to their redox and spin state, are routinely used to monitor the reaction. **Fig. 1** shows the absorption spectrum of dithionite-reduced bovine C*c*O. The heme absorption spectra (350-700 nm, **Fig. 1*a***) display empirically defined α-, β- and γ- (Soret) bands corresponding to the electronic and vibronic transitions from the same ground state to increasingly higher-energy excited states (**Fig. 1*b***). Platt`s convention [10] denotes the Soret band as B-band and groups the α- and β-bands into the Q- ("visible") band. The α- and γ-bands comprise two perpendicular electronic transitions each (Q_{0x}, Q_{0y} and B_{0x}, B_{0y}, respectively) oriented in the porphyrin plane (**Fig. 1*c***). Each of the four purely electronic transitions may have a vibronic satellite due to transition to a non-zero vibrational state (for example, B_{1y}, etc). The β-band comprises vibronic satellites of the α-band.

While heme *a* absorption dominates the Q-band, overlapping heme *a* and a_3 bands with high and similar intensities challenge spectral interpretation in the Soret. The Soret band of reduced bovine C*c*O shows a main peak at 443-444 nm accompanied by a shoulder at ~425 nm (**Fig. 1*a***). Our current knowledge of individual absolute spectra of hemes a^{2+} and a_3^{2+} relies on Vanneste's indirect derivation [11] based on variable-valence *vs* unliganded state spectral comparison referenced to the action spectrum of CO photodissociation from yeast C*c*O as the absolute spectrum of CO-bound heme a_3^{2+}. A 444-nm peak/~428-nm shoulder pair and a symmetric 442.5-nm peak (with a weak shoulder at ~420 nm) are therein respectively attributed to heme a^{2+} and heme a_3^{2+} (Fig. 5 in ref. [11] and **Fig. A.1**); these spectra are included in the textbooks and monographs (e.g. [12]). However, bovine C*c*O reduction kinetics analysis led Orii [13] to essentially opposite assignment of a featureless ~445-nm peak and the asymmetric band with a short-wavelength shoulder at ~428 nm to hemes a^{2+} and a_3^{2+}, respectively (see **Fig. A.1**).

In this work, we resolve individual absolute absorption spectra of the reduced bovine C*c*O hemes *a* and a_3 using two yet different approaches. First, we reconstructed the heme a^{2+}

spectrum from Ca^{2+}-induced spectral shift. Second, we selectively excited hemes a^{2+} and a_3^{2+} with femtosecond laser pulses and measured photobleaching spectra of the two hemes. Both approaches showed B_{0x}/B_{0y}-splitting in both hemes, heme a^{2+} transitions red-shifted relative to heme a_3^{2+} transitions, and the ~425 nm shoulder attributed mostly to heme a_3^{2+} spectrum.

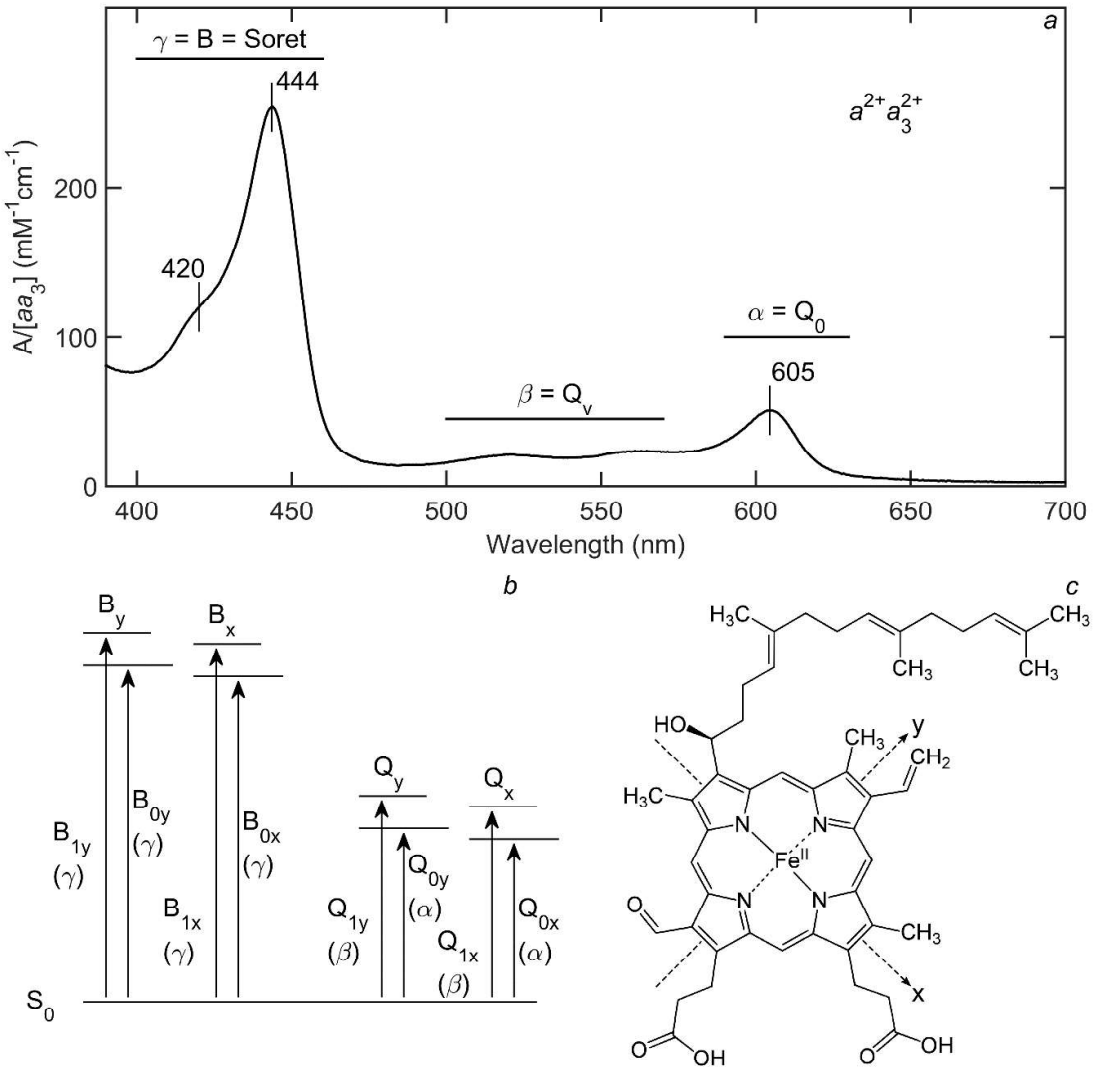

Fig. 1. Absorption bands of reduced cytochrome *c* oxidase. (*a*) experimental absorption spectrum of "activated" (see 2.1) C*c*O (1.7 μM) bovine C*c*O reduced by dithionite. (*b*) electronic (Q_{0x}, Q_{0y} and B_{0x}, B_{0y}) and first vibronic (Q_{1x}, Q_{1y} and B_{1x}, B_{1y}) transitions from the ground state S_0 corresponding to the α-, β- and γ- absorption bands for single hemes. (*c*) orientation of the x,y-transitions in the plane of porphyrin ring of heme A.

2. Materials and methods

2.1. Reagents and preparations. *aa*$_3$-type C*c*O was isolated from bovine heart mitochondria according to [14] modified as described in [15] and dissolved in 25-50 mM HEPES containing 0.05% DM. The concentration of the enzyme was determined from "dithionite-reduced *minus* oxidized" difference absorption spectra using an extinction coefficient $\Delta\varepsilon_{605-630}$ of 27 $mM^{-1}cm^{-1}$. Before KCN binding, C*c*O was "activated" as follows. Argon-deoxygenized ~30 μM C*c*O in 100mM HEPES/tris pH 8.0 was reduced by a small amount of dithionite in the presence of 20 μM of hexaammineruthenium ($Ru(NH_3)_6^{3+}$; RuAm) for 30 minutes until full reduction. Dithionite and RuAm were subsequently removed using centrifugal filter devices (Amicon Ultra-4, Millipore). *ba*$_3$-type C*c*O purified from *Thermus thermophilus* was prepared as described [16]. The concentration of the *ba*$_3$ C*c*O was determined using extinction coefficient $\Delta\varepsilon_{560-590}$ = 26 $mM^{-1}cm^{-1}$ for the absolute spectrum of the fully reduced oxidase [17]. Succinate-menaquinone reductase preparation was a generous gift from Prof. Lars Hederstedt (Lund University, Sweden). The concentration of the enzyme was determined from "dithionite-reduced *minus* oxidized" difference absorption spectra using an extinction coefficient $\Delta\varepsilon_{558-575}$ of 45 $mM^{-1}cm^{-1}$ [18].

2.2. Static spectroscopy. Absorption spectra were recorded in a Cary-300 Bio spectrophotometer in 1 ml quartz semi-micro cuvettes with a 1 cm optical path. A magnetic circular dichroism spectrum was recorded at room temperature in a quartz cuvette with a custom-built dichrograph (effective magnetic field ~ 0.7T for a 1 cm cell). The difference between direct and reverse magnetic field spectra was calculated to eliminate the contribution of the natural circular dirchroism.

2.3. Femtosecond selective photobleaching of the hemes. Multicolor pump-probe spectroscopy was performed with a setup based on a Quantronix Integra-C Ti-Saph oscillator/ amplifier system, delivering ~100 fs, 1.0 mJ pulses centered at 780 nm and operated at a repetition rate of 500 Hz. Pump pulses with different spectral characteristics (maxima at 623, 608, and 570 nm for the experiments with *aa*$_3$; 623 and 570 nm for the experiments with *ba*$_3$) with an energy of ~1 μJ were generated using a home-built, BBO-based (1 mm thick, θ=29.2°) type I non-collinear optical amplifier (NOPA [19]). The NOPA was pumped with pulses centered at 390 nm, generated by second harmonic generation of part of the 780-nm fundamental beam in a 1-mm θ=32° BBO crystal, and seeded with white light continuum generated by focusing part of the 780-nm beam on a 1 mm sapphire plate; the continuum was subsequently filtered appropriately using selected sharp edge interference filters (Semrock).

White light probe pulses were generated by focusing part of the fundamental on a 1 mm-thick CaF_2 window that was continuously translated perpendicular to the beam. The probe beam was dispersion-minimized around 435 nm by passing through a prism compressor, and then separated into the test and reference beams. After passing through the sample, the beams were dispersed and detected, shot-by-shot, on a CCD camera (Roper Scientific, SPEC-10) configured as a dual-array detector.

To mimic isotropic conditions, the polarization of the pump beam was set at 54.7° («magic angle») relative to polarization of the probe beam using a polarizer and a half-wave plate. To vary delay between the pump and probe pulses, the pump beam was passed through a delay line comprised of a retroreflector mounted on a step-motor driven translation stage. The 1-mm optical pathlength sample cell was rastered in a Lissajous scanner to ensure optimal exchange of the sample in the interaction volume. For every type of pump pulse, 10 spectrokinetics sets were recorded in the range 400-500 nm (spectral resolution ~1 nm) and with temporal steps of 83 fs from -1 to 2 ps and of 2 ps from 2 to 50 ps. Due to dispersion the effective zero time depended on the wavelength, varying the onset of the absorption changes for up to 700 fs. We accounted for this dispersion during data processing.

2.4. Preparation of the samples for the femtosecond spectroscopy. Enzymes were diluted in 200 mM HEPES/Tris buffer, pH ~ 7, with 0.05% DM dodecylmaltoside and 0.5 mM Na-EDTA. Quartz cuvettes with a 1 mm optical pathway ("Hellma-Analytics"), type 110-QS were filled with the sample and hermetically closed with plug-type rubber sleeve stoppers ("Kimble", USA). C*c*O and succinate: menaquinone reductase (SMR) were reduced with a fresh 0.2M sodium dithionite solution (final concentration ca. 1-5 mM dithionite). To prepare the dithionite solution, degassed MilliQ was added to degassed dithionite powder into an argon-filled vial. The sample in the cuvette was degassed with a vacuum pump and the volume above the sample was saturated with argon. Dithionite was added through the stopper using a Hamilton syringe, and the volume above the sample was again saturated with argon. Reduction was considered complete if the absorption spectrum corresponded to the reduced form (in the case of C*c*O showing maxima at 444 nm and 605 nm) and stayed unchanged for at least 10 minutes. The absorption in the Soret band of the reduced form was 0.8-1.0 OD.

2.5. Data analysis. Global analysis of the pump-induced absorption changes was performed using Glotaran software [20] to extract the fastest evolution-associated spectra (EASs) with correction for the instrumental response function, zero-time dispersion and

coherent artifacts. Prior to global analysis, noise in the data was reduced using singular value decomposition. Relaxation included typically three phases with characteristic times of ca. 0.2, 1 and 5 ps, the fastest component representing photobleaching. Additional components did not improve the fit. Decompositions into gaussians were performed in MATLAB using the 'Interior-point' algorithm [21–23] to minimize the mean square difference between the experimental and simulated curves.

3. Results

3.1. Reconstruction of heme a^{2+} absorption bands using Ca^{2+}-induced spectral shift. In C*c*O from vertebrate mitochondria, a specific cation-binding site in subunit I near heme *a* and Cu_A reversibly binds Ca^{2+} and Na^+ ions [24–26]. Ca^{2+} red-shifts the entire heme *a* absorption spectrum by ~1 nm [24,27]. The shift is small compared to the linewidths of the heme a^{2+} absorption bands, so the difference spectrum of the shift represents the differential of the absolute a_3-free heme a^{2+} spectrum, and can be used to derive the heme a^{2+} absolute spectrum lineshape [28].

We first compared the Ca^{2+}-induced spectral shift in the fully reduced unliganded complex $a^{2+}a_3^{2+}$ and the mixed-valence cyanide complex $a^{2+}a_3^{3+}$-CN (**Fig. 2*a*,*b***). In contrast to absolute spectra (**Fig. 2*a***), the Ca^{2+}-induced difference spectra (**Fig. 2*b***) for these two states are virtually identical both in the Soret and the visible. This finding confirms that heme a^{2+} is a unique contributor to the Ca^{2+}-induced spectral changes. Thus, the non-zero a_3^{2+} contribution put forward earlier [24] is not supported by our data obtained using a more stable reduction system. It also shows that the heme *a* spectrum is not affected by the redox and spin state of heme a_3.

We chose the $a^{2+}a_3^{3+}$-CN complex as the starting point to better separate the overlapping γ-peaks and minimize any possible interference from heme a_3. The absolute $a^{2+}a_3^{3+}$-CN spectrum (**Fig. 2*a***, black) showed a split Soret band with maxima at 442 nm and 430 nm (mainly heme a^{2+} and heme a_3^{3+}-CN, respectively) and rather symmetric α-band at 605 nm.

The corresponding difference spectrum (**Fig. 2*b***, black) is dominated by narrow 1st – derivative-like features in the Soret and in the visible. The Soret band signal shows A_{min} at 438 nm, A_{max} at 460 nm and a zero-crossing point at 449 nm, that coincides with neither of the two maxima in the parent absolute spectrum. An inflection around the zero-crossing point

suggests juxtaposition of two overlapping 1st derivative-shaped components [24,28]. In the visible, the difference spectrum shows the zero-crossing point at 605 nm, close to the maximum of heme a^{2+}. A small derivative-shaped feature centered around 520 nm may correspond to a red shift of the β-band of heme a^{2+}.

The integral of this differential spectrum in **Fig. 2*b*** gives the reconstructed lineshape of the heme a^{2+} absolute spectrum (**Fig. 2*c***, black). A weak baseline (**Fig. 2*b***, green dotted line) was subtracted from the difference spectrum before integration to avoid negative values in the reconstructed spectrum. We decomposed the spectral lineshape into a sum of gaussians with the following assumptions:

(1) the Soret and α-band are comprised of two individual electronic transitions (cf. **Fig. 1*b,c***);

(2) the x and y transitions can be degenerate or non-degenerate in energy;

(3) The x and y transitions of the same band must have equal linewidths, but their intensity ratio may vary;

(4) Bands in 500-580 nm region are approximated by two gaussians of variable linewidths.

The reconstructed heme a^{2+} Soret band with a maximum at 447.5 nm is symmetric and much narrower than reported by Vanneste (full width at half-height (FWHH) 18 nm vs 24 nm, correspondingly [11]). It is described by the sum (**Fig. 2*c***, red) of two gaussians of equal FWHH of 15 nm at 442 nm and 450 nm, and an additional minor component at 420 nm with a FWHH of 18 nm (red dotted). We assign the gaussians at 442 and 450 nm to two non-degenerate B_y and B_x electronic transitions in heme a^{2+}, split by 8 nm, respectively.

Short-wavelength components of the heme a^{2+} Soret band could reside, in principle, below 420 nm. However, most conventional reductants such as dithionite or ascorbate strongly absorb in the near-UV possibly masking these spectral components. We therefore attempted to obtain a "clean" spectrum of C*c*O in the Soret band by bubbling gaseous hydrogen *in statu nascendi* released by sodium borohydride through the anaerobic solution of the oxidized enzyme. Hydrogen bubbling resulted in partial (~85%) C*c*O reduction. The H_2-reduced C*c*O spectrum corrected for the fraction of the oxidized form (**Fig. 2*d***) reveals no additional spectral components below 420 nm.

The splitting of the Soret band of heme a^{2+} implies that the α-band of the heme should similarly contain split x- and y- components [29]. The α-band differential Ca^{2+}-induced spectrum shows certain asymmetry (**Fig. 2*b***), and, consistently, the reconstructed α-band

(maximum at 605 nm, FWHH 21 nm) has somewhat extended short wavelength side. The α-band fitting requires two gaussians of 17-18 nm FWHH separated by 13 nm (at 593 nm and 606 nm). However, in variance with the Soret band, the x and y components of the Q_0-band differ much in intensity, so that the overall maximum at 605 nm almost coincides with the maximum of the dominating Q_{0x}-transition at 606 nm.

To further explore the proposed Q_0-band splitting, we recorded room temperature magnetic circular dichroism (MCD) spectrum of our C*c*O preparation in the visible range (**Fig. 2*e***, black). The spectrum with positive and the negative lobes at 609 nm and 590 nm and zero-crossing at 600 nm is very close to that in [29], except for a slight shift of our spectrum to the red. The MCD spectrum decomposes into a sum of two gaussians of equal magnitude and width but of opposite sign corresponding to the individual heme a^{2+} Q_{0x} and Q_{0y} terms, and a third negative gaussian at 574 nm (**Fig. 2*e***, red dashed: gaussians, red solid: their sum). The extrema of the two components are observed at 594 (min) and 605.5 nm (max), *i.e.,* very close to the maxima of the two components fitted to the heme a^{2+} α-band (**Fig. 2*c***), supporting their attribution to the Q_{0x}- and Q_{0y}- electronic transitions.

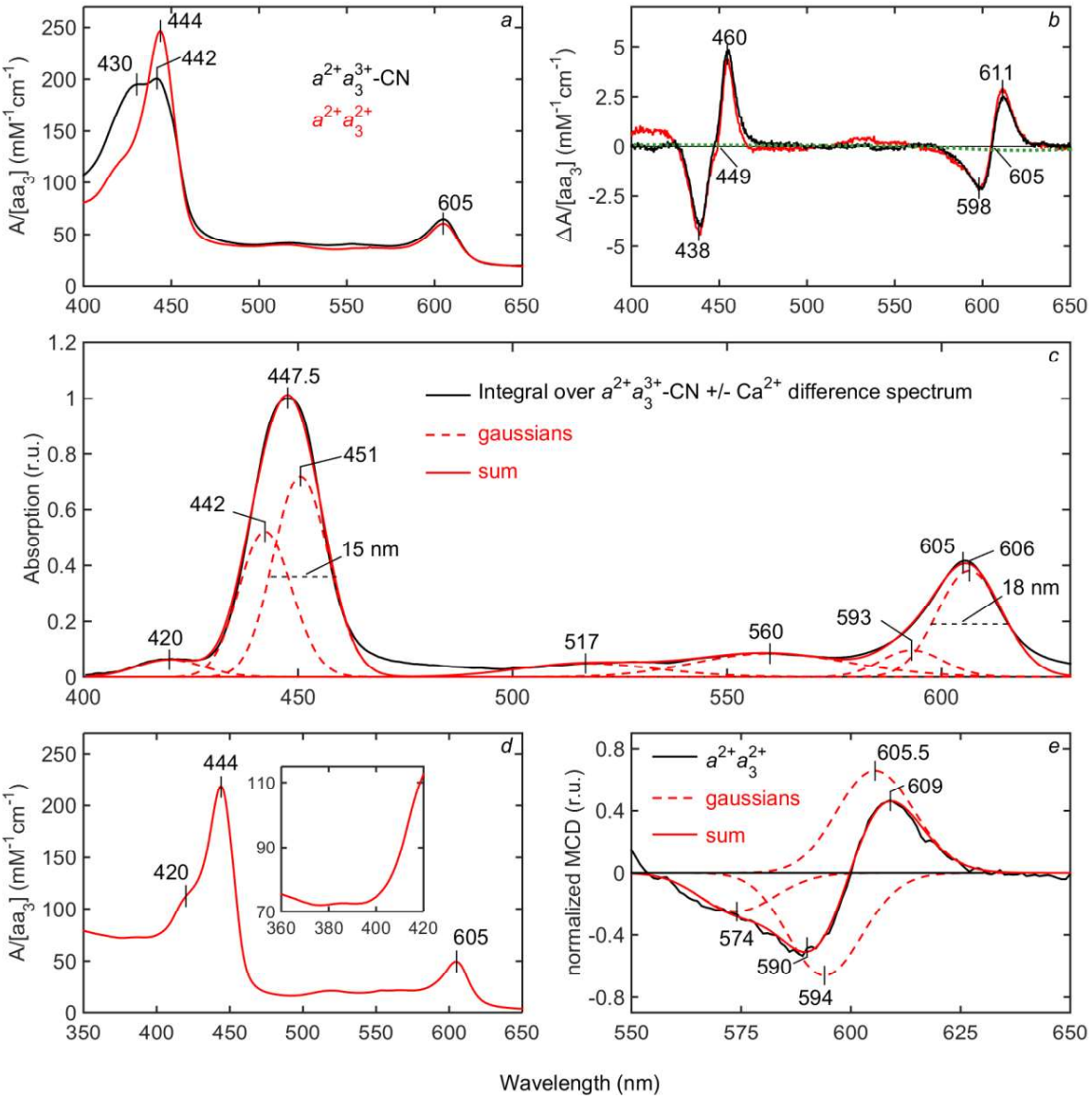

Fig. 2. Reconstruction of the heme a^{2+} absorption spectrum using selective Ca^{2+}-induced spectral shift. (*a*) Absorption spectra of the bovine C*c*O: black, mixed-valence CN-complex $a^{2+}a_3^{3+}$-CN; red, fully reduced unliganded enzyme $a^{2+}a_3^{2+}$. To obtain the mixed-valence CN-complex, "activated" (see 2.1) C*c*O (1.7 μM) in the basic medium was incubated for 10 minutes with 4 mM KCN and then reduced by 5 mM Tris-ascorbate in the presence of 100 μM TMPD. To produce fully reduced form, C*c*O was incubated with 5 mM ascorbate and 50 μM RuAm, in a cell covered by a gastight cap. Anaerobic condition followed by full enzyme reduction were achieved after 5-min incubation. (*b*) Difference spectra of the Ca^{2+}-spectral shift of heme *a*. The curves show the difference between the absolute spectra of the C*c*O mixed-valence CN-complex (black) or fully reduced form (red) after the addition of 0.1 mM

$CaCl_2$ and after the subsequent addition of 1 mM EGTA. With the adventitious calcium in the buffer (~ 30 µM), the Ca^{2+} concentration after $CaCl_2$ addition was ~130-fold the K_d value [26], i.e., sufficient to saturate the calcium binding site. (*c*) Reconstructed lineshape of the heme a^{2+} absorption spectrum. Black, integral over the black curve in *b*. Red, its approximation by the sum of seven gaussians (dashed red). (*d*) H_2-reduced bovine C*c*O absoption spectrum corrected for the contribution (~15%) of resting oxidized form. The spectrum shows no additional shoulder below 420 nm. *Insert*: zoom of the 360-420 nm region. (*e*) Black, MCD spectrum of reduced bovine C*c*O. Red, its approximation with 3 gaussian components (dashed red). To obtain reduced C*c*O, 50 µM $Ru(NH_3)_6^{3+}$ and 5 mM ascorbate was added to 12 µM C*c*O in 0.1M HEPES pH 8.1 with 0.1 mM of added Ca^{2+}, 5 minutes prior to the recording of the spectrum.

3.2. Individual spectra of hemes in the T. thermophilus ba_3 and mitochondrial aa_3 CcO resolved with photoexcitation spectroscopy. Independently, we employed a selective photobleaching approach [30–33] by exciting the hemes by a femtosecond light pump pulse in the Q band to transiently depopulate the electronic ground state and thus to bleach the corresponding ground state-based absorption. Spectral changes were followed using a white continuum probe pulse. Since both Q and B bands originate from the same ground state, excitation in the Q-band bleaches in the Soret as well. Wide separation of the two bands prevents interference of the relatively narrow pump pulse in the Q-band with the probe pulses in the Soret.

However, the heme a^{2+} and heme a_3^{2+} Q-band overlap and finite intrinsic width of the pump pulses complicates selective excitation of one heme. Therefore, we turned initially to *T. thermophilus* ba_3-type C*c*O belonging to the same heme-copper superfamily as the aa_3-type oxidases but with heme *b* instead of heme *a*. In the ba_3-type C*c*O, the Q-bands of high-spin heme a_3^{2+} (~613 nm) and low-spin heme b^{2+} (559 nm) are separated better than the Q-bands of bovine C*c*O hemes *a* and a_3 (**Fig. 3a,*b***). The Soret bleaching only occurs if the pump pulse overlaps with the visible absorption bands. Pumping at 570 nm is expected to excite both hemes and results in photobleaching spectrum with maximum at 426 nm (heme b^{2+} band) with a weak feature at 443 nm (putative heme a_3^{2+} band) **(Fig. 3*c***). In contrast, the pump pulse at 623 nm ("623exc" condition) (**Fig. 3*b***, red) is expected to selectively excite heme a_3^{2+} since it does not overlap with the heme b^{2+} narrow α-band at 559 nm. Compared to the spectrum of heme a^{2+} in the bovine C*c*O (**Fig. 2*c***), 623exc photobleaching spectrum **(Fig. 3*d***) is blue-shifted and strongly asymmetric with extended decay on the high-energy side. Besides two equal-width (12 nm) gaussians at 435 and 444 nm assigned to the purely electronic B_{0y}- and B_{0x}- transitions, the fitting requires a wider band at ~427 nm that may represent the sum of vibronic components. The absence of 623exc photobleaching of *Bacillus subtilis* reduced succinate: menaquinone reductase (SMR) containing heme *b* as the only bleaching target [34] rules out potential heme *b* contribution to this 427-nm band (**Fig. 3*d***).

Due to spectral overlap, the photobleaching of individual aa_3 C*c*O hemes cannot be resolved with single excitation. We therefore used three excitation wavelengths to vary the heme a^{2+} *vs* heme a_3^{2+} excitation degree. **Fig. 4*a*** shows dithionite-reduced aa_3 photobleaching spectra obtained by excitation with pump pulses centered at 570, 608 and 623 nm ("570exc", "608exc" and "623exc"). The 608exc spectrum qualitatively resembles the C*c*O photobleaching spectrum reported recently for a similar pump-probe protocol with the

excitation at 600 nm [35,36]. The “570exc”, “608exc” and “623exc” spectra differ in amplitude since the photoexcitation yield depends on the absorption strength in the region of excitation and on the pump energy. However, their lineshapes also differ, suggesting varying degree of a^{2+} vs. a_3^{2+} excitation selectivity. The 623exc lineshape is almost symmetrical with a minor shoulder below 430 nm. The shoulder contributes more to 608exc and especially 570exc spectra. The maximum of the 570exc spectrum is slightly blue-shifted (see **Fig. 4*a***, color traits). As the heme a_3^{2+} ground state absorption spectrum is blue-shifted relative to heme a^{2+} spectrum (cf. **Fig. 2*c*** and **Fig. 3*d***), the blue shift of the maximum on the 570exc spectrum provides a first indication that heme a_3^{2+} contributes more to the 570exc spectrum than to the 608exc and 623exc spectra.

To estimate the excitation selectivity, we convoluted the pump pulse positions with the Q-bands of the hemes a^{2+} and a_3^{2+} (**Fig. 4*b***). The spectrum reconstructed from the Ca^{2+}-induced shift assay was used to model the heme a^{2+} Q-band, assuming that heme a^{2+} contributes about 80% of absorption in the α-band maximum. The heme a_3^{2+} Q-band was modeled by subtraction of the heme a^{2+} spectrum from the smoothened aa_3 Q-band. The resulting a_3^{2+} spectrum has a maximum at ~600 nm and a shoulder below 580 nm, consistent with the reduced minus oxidized heme a_3 spectrum [37] (see also **Fig. A.5**). We then estimated the heme a^{2+} *vs*. heme a_3^{2+} selectivity as the convolution of the pulse profile with the heme a^{2+} absorption band divided by a convolution of the same pulse profile with the heme a_3^{2+} absorption band:

$$a : a_3\ selectivity\ = \frac{\int I_a(\omega) I_{pulse}(\omega)}{\int I_{a_3}(\omega) I_{pulse}(\omega)}, \qquad (1)$$

where I_a and I_{a3} are heme a^{2+} and heme a_3^{2+} Q-bands, respectively, I_{pulse} is the corresponding pump pulse profile (570exc, 608exc or 623exc), and the integrals are taken over the 15391-19992 cm^{-1} spectral range (500-650 nm).

The estimated a^{2+} *vs*. a_3^{2+} excitation yield ratios (**Fig. 4*b***) suggest a higher contribution of heme a^{2+} to the photobleaching spectra at 623exc and 608exc and approximately equal a_3^{2+} and a^{2+} contributions at 570exc. However, under any excitation conditions, it was not possible to assign the photobleaching spectra entirely to either heme a^{2+} or a_3^{2+}. To extract “pure” hemes a^{2+} and a_3^{2+} spectral lineshapes we performed simultaneous decomposition of the photobleaching spectra obtained at all three excitations (**Fig. 4*c*-*e***) with the following constraints:

.(1) The Soret (*B*-) band of each heme is modeled by 3 gaussian components: two electronic transitions (B_{0x}- and B_{0y}-) with equal widths plus a putative vibronic satellite of variable width. The three gaussians describing heme a^{2+} and heme a_3^{2+} contributions are shown in **Fig. 4*c-e*** by orange and green, respectively.

(2) Position and bandwidth in cm^{-1} (but not amplitude) of a specific transition within a heme is identical for all three photobleaching spectra. For example, the heme a^{2+} B_{0x}-associated gaussians are centered at the same wavelength and have the same width in each of the three sets of gaussians but may differ in amplitude.

(3) The resulting shape of the spectrum of an individual heme (a^{2+} or a_3^{2+}) is preserved across the excitation conditions. For example, the sums of the three gaussians attributed to heme a^{2+} have the same lineshape for each of the three sets of gaussians but may differ in amplitude.

(4) The photoinduced absorption is simulated by two negative gaussians, one at either side of the spectra, whose positions and bandwidths in cm^{-1} were identical across the excitation conditions.

The "pure" normalized heme a^{2+} photobleaching spectrum (**Fig. 4*f***, solid orange) is in agreement with the spectrum obtained using Ca^{2+}-induced shift approach (**Fig. 4*f***, gray, same as **Fig. 2*c***, black). It reveals almost symmetrical lineshape with minor shoulder at 421 nm and contains two individual gaussian components with maxima at 442.5 nm and 450 nm, with a bandwidth of 14 nm each. In contrast, the "pure" normalized heme a_3^{2+} photobleaching spectrum **(Fig. 4*g*)** has a pronounced shoulder described by 423 nm band with a 25 nm width. In both hemes *a* and a_3, the B_x- and B_y- electronic transitions are separated by ~8 nm.

As a consistency check, we attempted to reconstruct the overall $a^{2+}a_3^{2+}$ Soret band as a weighted sum of the individual a^{2+} and a_3^{2+} contributions. First, we estimated the proportion of the heme a^{2+} vs. heme a_3^{2+} contribution by assuming that the a:a_3 excitation selectivity is most reliably estimated for 608exc condition, where the pumping is close to the heme a^{2+} band maximum (**Fig. 4*b***). Selectivity modeling suggests that pumping at 608 nm excites heme a^{2+} 3.15 times stronger than heme a_3^{2+}. At the same time, the ratio of the areas under the sum of the gaussians attributed to heme a^{2+} (orange) to that under the sum of the gaussians attributed to heme a_3^{2+} (green) on the 608exc is not 3.15:1 but 1.70:1 (**Fig. 4*d***). This could mean that the contributions of the two hemes to the total extinction are not 1:1 but rather 0.54:1 (heme a^{2+}: 35%, heme a_3^{2+}: 65%). The ratio of the areas under the sums of the heme a^{2+} and heme a_3^{2+}-assigned gaussians for 570exc and 623exc fits (predicted

selectivities 0.77 and 4.95, respectively) are 0.58:1 and 2.55:1. This gives the following estimates of the hemes' contributions to the extinction: 43% (heme *a*) and 57% (heme a_3) for 570exc fit; 34% (heme *a*) and 66% (heme a_3) for 623exc fit. The both estimations are fairly close to that obtained above for the 608exc data which confirms the consistency of our modeling.

Finally, we obtained the reconstructed aa_3 Soret lineshape (**Fig. 4*h***, red) by adding the normalized heme a^{2+} spectrum multiplied by 0.54 to the normalized heme a_3^{2+} spectrum multiplied by 1, and normalizing the sum to its maximum. For comparison, the dithionite-reduced aa_3 spectrum is shown, also normalized to its maximum (**Fig. 4*h***, gray). The reconstructed Soret lineshape reproduces the position of the maximum and the shoulder at the short-wavelength side. We then investigated whether scattering may explain higher experimental absorption below 430 nm compared to the reconstructed spectrum. For this, we added $\sim\lambda^{-4}$ absorption (**Fig. 4*h***, dotted dark red curve) to the sum of $a^{2+}$and a_3^{2+} bands. The maximum-normalized resulting spectrum (**Fig. 4*h***, dotted blue curve) is fairly close to the experimental Soret lineshape. The remaining differences between the reconstructed band and the experimental $a^{2+}a_3^{2+}$ spectrum can be due to imprecise description of the vibronic satellite(s) by unique gaussian band, unaccounted higher-energy heme transitions, and the β-band tails. Attempting more precise Soret band reconstruction, as well as determination of absolute heme absorbance values, is out of the scope of the present work.

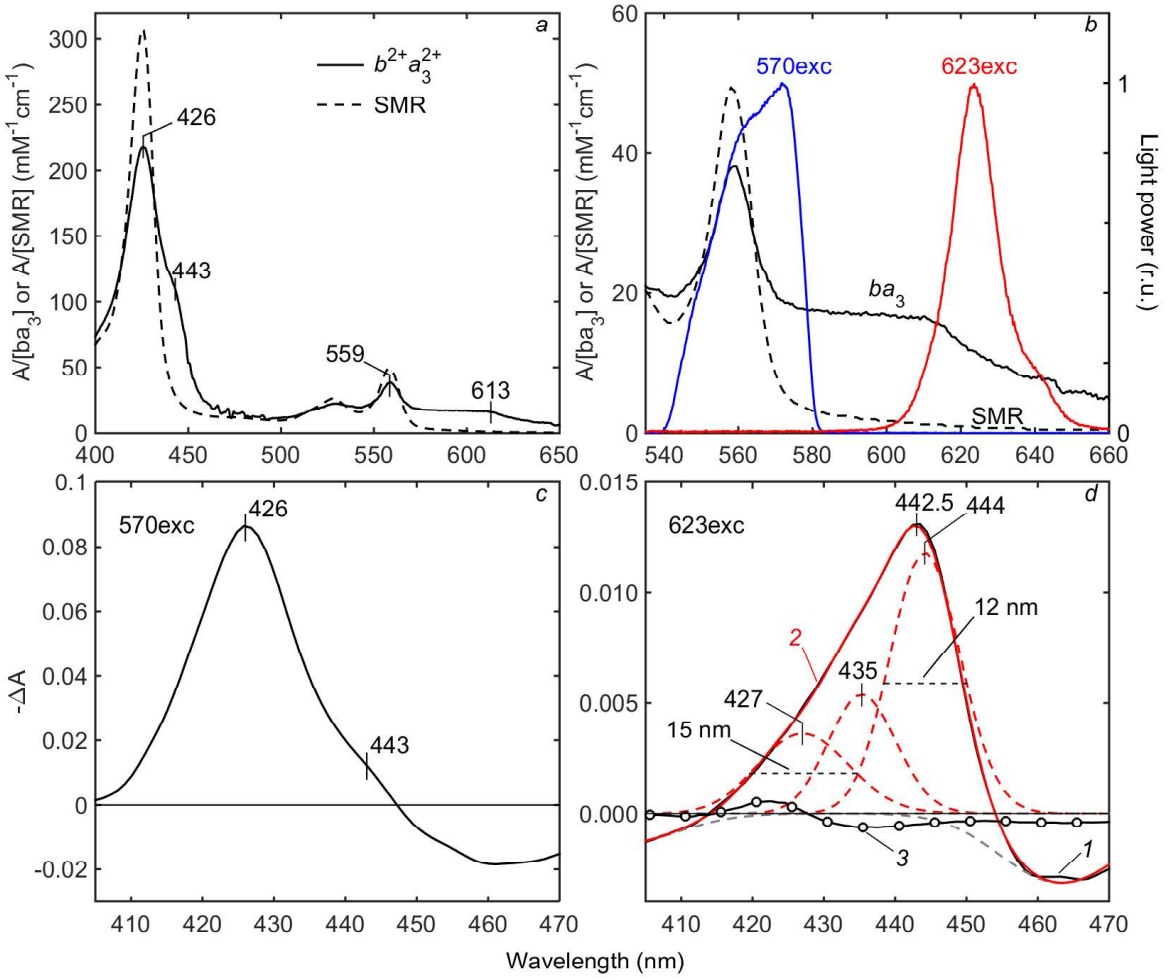

Fig. 3. Photobleaching of reduced *ba*$_3$ C*c*O from *T. thermophilus*. (*a*) Dithionite-reduced *T. thermophilus ba*$_3$ (7.9 μM; solid) and *Bacillus subtilis* succinate: menaquinone reductase (SMR, 4.1 μM; dashed) absorption spectra. (*b*) Pump laser pulse profiles (right vertical axis) centered at 570 nm (blue) and 623 nm (red) relative to the α-band of the reduced *ba*$_3$ spectrum (black, left vertical axis). The *B. subtilis* SMR spectrum (dashed) does not overlap with the 623exc pulse profile suggesting that heme b^{2+} is not excited by this pulse. (*c,d*) Inverted fastest EASs after pumping at 570exc and 623exc, respectively. In *d*, Curve *1* (solid black), experimental spectrum that has been fitted by 5 gaussians. The 3 positive gaussians (dashed red) are assigned to heme a_3^{2+} photobleaching. Two negative gaussians (dashed gray) approximate the increase of absorption following the excitation that likely represent the contribution of the electronically excited states (typically weak and diffuse) [38–40]. Curve *2* (solid red) shows the sum of the 5 gaussians mostly coinciding with the experimental curve *1*. Curve *3* (black with open circles), control experiment showing that heme b^{2+} in *B. subtilis* SMR is not photobleached by excitation at 623 nm.

425

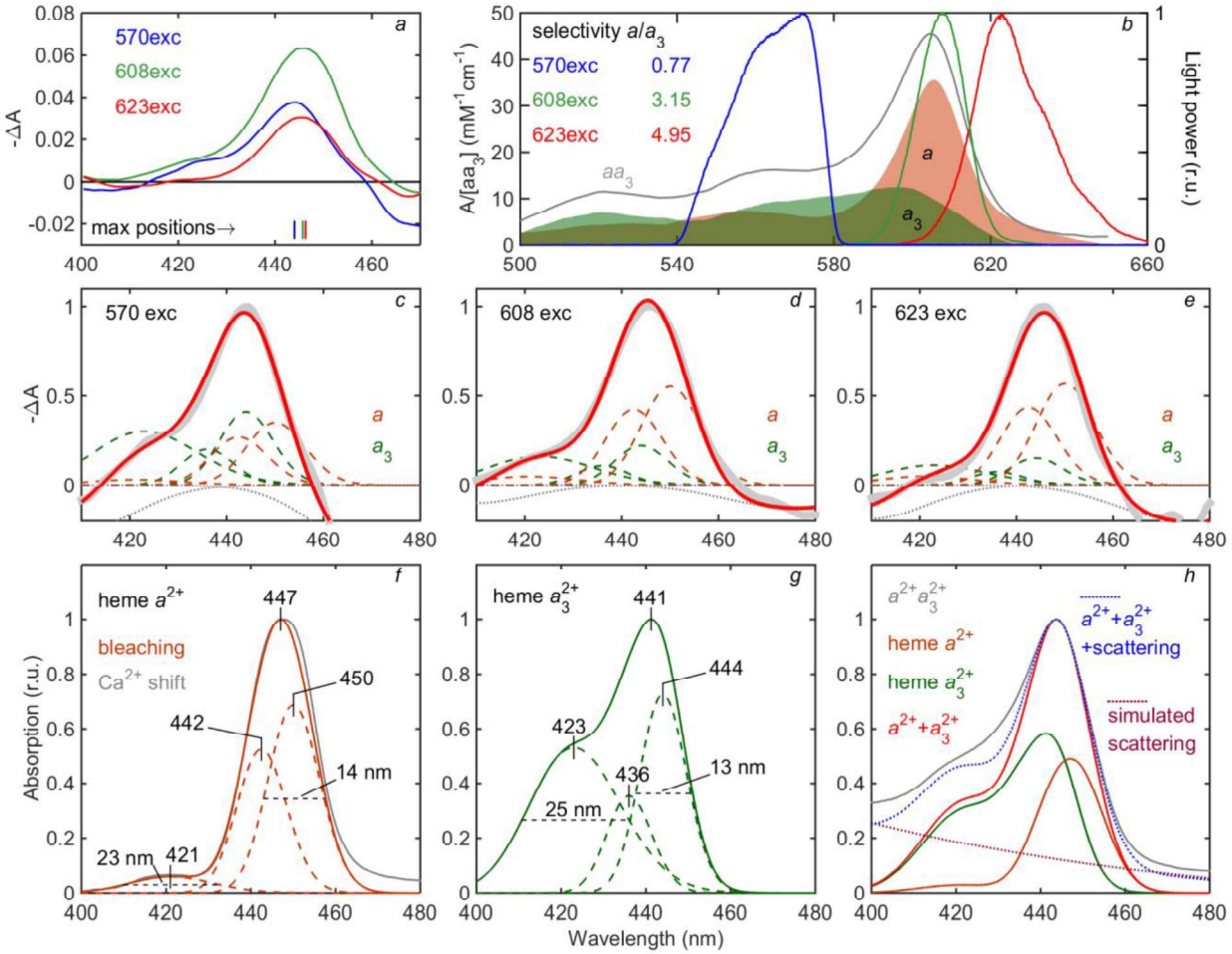

Fig. 4. Photobleaching of reduced bovine C*c*O. (*a*) Inverted fastest EASs after pumping at 570, 608 and 623 nm. The traits at the bottom show corresponding maxima positions. (*b*) Heme a^{2+} *vs.* heme a_3^{2+} excitation selectivity estimation. Heme a^{2+} spectrum (red area) reconstructed from the Ca^{2+}-induced shift (**Fig. 2*c***) was subtracted from the smoothened reduced *aa*$_3$ spectrum (gray) to model heme a_3^{2+} spectrum in the visible range (green area). Heme a^{2+} was assumed to provide ~80% absorption at the α-band maximum. The pump pulse profiles for 570exc, 608exc and 623exc are shown in blue, green and red, respectively. Excitation selectivity was estimated using Eqn (1). (*c*-*e*) Approximation of the EASs (thick gray lines) by sets of 6 positive (dashed) and 2 negative (dotted) gaussians. In each fit, three positive gaussians were attributed to heme a_3^{2+} (green) and the other three to heme a^{2+} (orange). The two negative gaussians describe photoinduced absorption. The sum of the gaussians is shown by a solid red line. (*f,g*) Heme a^{2+} and heme a_3^{2+} Soret lineshapes (solid lines) determined from the EASs fitting as sums of the three corresponding gaussians

(dashed lines). The lineshapes are normalized to their maxima. In *f*, heme a^{2+} Soret lineshape determined with Ca^{2+}-induced shift technique (gray) is shown for comparison. (*h*) Bovine $a^{2+}a_3{}^{2+}$ Soret lineshape reconstruction. The ratio of the areas under scaled Soret bands of hemes a^{2+} and $a_3{}^{2+}$ (orange and green) was estimated to be a^{2+}:$a_3{}^{2+}$=0.54:1 (see Section 3.2). Red, the sum of the individual a^{2+} and $a_3{}^{2+}$ contributions normalized to its maximum. Dotted dark red, simulated ~λ^{-4} scattering. Dotted blue, the sum of reconstructed a^{2+} and $a_3{}^{2+}$ bands and the scattering normalized to its maximum. Gray, Soret band of the dithionite-reduced bovine C*c*O normalized to its maximum.

4. Discussion

Table 1 resumes heme a^{2+} and a_3^{2+} spectral properties reported here and compares them with previous studies. Only two papers treat explicitly the lineshape of the absolute spectra of bovine C*c*O hemes a^{2+} and a_3^{2+}: Vanneste's [11] and Orii's [13]. Our spectra coincide with neither of the two reports but would appear closer to Orii's conclusions. However, the latter depend critically on the choice of the model parameters and can be converted into Vanneste's attributions by changing the baseline slope (**Fig. A.2**). It has been shown by using improved reduction technique that Vanneste's heme a_3 spectra need to be corrected at least in the α-region [37]. In the following we will discuss the spectral properties of the two hemes in detail.

4.1. Soret splitting. Both hemes a^{2+} and a_3^{2+} showed split Soret bands with B_{0x}- and B_{0y}-components separated by 8-9 nm and close electronic transition widths. The heme a^{2+} Soret band splitting has been inferred earlier [28,29,41–43], but sometimes misinterpreted as evidence for two heme *a* conformations [42]. The hemes *a* and a_3 in C*c*O have the same chemical structure - heme A, - but differ in the protein surroundings and in iron coordination. Therefore, the simplest explanation is that the similar splitting observed for the two hemes is intrinsic to heme A structure. Indeed, the electronic transition along the pyrrole II → pyrrole IV axis with the two electron-withdrawing substituents (vinyl and formyl) should differ in energy from the perpendicular transition along the pyrrole I → pyrrole III axis with electron donating substituents (methyl, propionate, hydroxyethylfarnesyl group). Conversion of the formyl substituent to the Schiff-base results in drastic narrowing of the heme A Soret band [44] (see also **Fig. A.3**) suggesting restoration of degeneracy or at least reduction of splitting. Inherent heme A splitting is supported by the MCD spectrum of the bis-1-methyl imidazole-6c complex of heme A^{2+} showing the same lineshape (except for the position) as the C*c*O heme a^{2+} MCD spectrum [29]. However, it seemingly contradicts the absorption spectra second derivative analysis (cf. [41] and refs. therein) suggesting that the Soret splitting is specific for heme a^{2+} in C*c*O and is not observed in the hexacoordinate (6c-) low-spin (ls-) complexes of isolated heme A^{2+} nor in non-*a*a_3-C*c*O proteins reconstituted with heme *a*.

To clarify this issue, we first tested whether deconvolution into gaussians can reveal the Soret splitting of the isolated heme A^{2+} spectrum by analyzing the bis-imidazole-heme A^{2+} spectra reported in [44]. The ls-6c-heme A^{2+} spectra in solution are broader than in C*c*O (35 nm in aqueous buffer or 27 nm in CH_2Cl_2 *vs* 18 nm in the C*c*O protein) and, at this width, single- and two-gaussian approximations (both including one additional gaussian describing a

vibronic shoulder) are equally valid (**Fig. A.3**). Further, simple modeling (**Fig. A.4**) shows that the ~10-nm splitting of two gaussians with equal heights and widths typical for C*c*O requires their FWHH being below ~8 nm to be detected on the second derivative curve. The exact lineshape of the second derivative depends also on the relative heights of the two gaussians. Thus, the second-derivative method may resolve the B_{0x} and B_{0y} bands of heme *a* in the CO-complex of reduced C*c*O, with heme a_3 bands shifted far to the blue (cf. Fig. 1B in [41]) and to a lesser extent in the fully reduced C*c*O (Fig. 1A in ref. [41]), but is not expected to resolve the B_{0x}- and B_{0y}- bands in the broad spectra of the isolated 6c-heme A^{2+}.

The same applies to the recent second-derivative analysis of the Soret C*c*O spectra confirming ferrous heme *a* Soret splitting but arguing against splitting of the ferric hemes *a* and a_3 Soret bands [45]. On this basis, the authors proposed that the ferric hemes are symmetric but their reduction changes the protein conformation distorting heme planes and splitting the B_{0x}- and B_{0y}-transitions. However, the Soret bands of the ferric hemes are known to be broader than those of the reduced hemes and their splitting may be unresolved by the second derivative assay.

We conclude that although not detectable by second-derivative analysis, the inherent splitting of the heme A^{2+} Soret band is in the origin of the Soret band splitting of both hemes a^{2+} *and* a_3^{2+}.

4.2. Heme a^{2+} *α-band splitting.* Spectral forms of heme a^{2+} differing in the *α*-peak were described [46,47] but the possibility of a split *α*-band of the heme was not considered in these studies. Our analysis revealed the presence of a second minor component at 593 nm in addition to the dominating band at 606 nm (**Fig. 2*c***). Their attribution to the split Q_{0y} and Q_{0x} bands of heme a^{2+}, respectively, is supported by MCD spectroscopy that allows for better resolution of the split bands. The *α*-band heme a^{2+} MCD spectrum can be interpreted as a sum of two opposite B-terms belonging to the Q_{0x} and Q_{0y} transitions in heme a^{2+} [29]. The MCD spectrum of our preparation is indeed described as the sum of two identical B-terms of opposite signs (**Fig. 2*e***).

The Soret splitting is more extensive than that of the *α*-band (381-416 *vs* 373 cm^{-1}) probably due to the larger Soret *vs α*-band transition moment implying stronger interaction with the permanent local electric field [48]. In contrast to the Soret where the B_{0x}/ B_{0y} intensity ratio is about 1.4 (see **Table 1**), the Q_{0y} band at 593 nm is much weaker than the Q_{0x} component at 606 nm (absorption intensity ratio Q_{0x}/Q_{0y} is ~4). The weaker high-energy (y) Q_0-component is typical of metal-porphyrin compounds with split absorption bands [49–53]

and agrees with calculations [50,54]. Therefore, the commonly observed *α*-peak of heme a^{2+} at 605 nm largely corresponds to the Q_{0x} transition of the iron-porphyrin ring of heme a^{2+}.

4.3. Position of the Soret absorption peaks of the hemes a^{2+} and a_3^{2+}. It is commonly assumed that the Soret absorption maxima of hemes a^{2+} and a_3^{2+} are close to each other (Vanneste: 444 nm a^{2+} vs 443 nm a_3^{2+} [11]; Orii: 445 nm a^{2+} vs 443 nm a_3^{2+} [13]). This fact has been long considered surprising in view of the difference in iron coordination and heme-protein interaction.

Our data, in contrast, suggest that the Soret maxima (447-447.5 nm a^{2+} vs 441 nm a_3^{2+}) and the B_{0x}-, B_{0y}-transition energies of hemes a^{2+} and a_3^{2+} do actually differ. The heme a_3^{2+} B_{0x}- and B_{0y}-transitions are shifted by 6-7 nm to the blue relative to the corresponding transitions of heme a^{2+}, in agreement with the blue shift of the reduced minus oxidized difference spectrum of C*c*O heme a_3 relative to that of heme *a* [37]. In apparent contradiction, Soret maxima of high spin mono-His-coordinated (5c-hs) cytochromes *b* are usually situated to the red from those of low spin, bis-His-coordinated (6c-ls) cytochromes *b* (**Table A.1**). Congruently, the wide α-band of 5c-hs 1,2-diMeIM-heme A^{2+} (heme a_3^{2+} model) locates to the red of the α-band of 6c-ls bis-1-MeIm-heme A^{2+} (heme a^{2+} model) [29,41,44]. The inverted maxima positions in C*c*O may be explained by the opposite shifts of the C*c*O hemes relative to the corresponding isolated complexes. The spectrum of C*c*O heme a^{2+} is red-shifted by 9-11 nm in the Soret and by 12-16 nm in the α-band compared to the 6c-ls bis-1-MeIm-heme A^{2+} (**Table 1**). This shift is probably induced by a strong hydrogen bond between the in-plane oriented heme *a* formyl group and the conserved arginine $R38_{bt}$ as proposed originally in [55] and confirmed by mutagenesis of the homologous arginine in bacterial C*c*Os [56,57]. Indeed, the replacement of the homologous arginine to methionine causes a 605 nm to 589 nm shift of the α-band that would correspond to ~10 nm shift in the Soret [56]. On the other hand, the reduced *minus* oxidized difference spectrum of the C*c*O heme a_3 appears to be blue-shifted by about 7 nm compared to that of 5c-hs heme A^{2+} while preserving the spectral shape ([37]; **Fig. A.5**) suggesting ~3-4 nm blue shift in the Soret.

4.4. B-band short-wavelength shoulder. Heme a_3^{2+} shows a pronounced high-energy shoulder of the Soret peak (**Fig. 4*g***), presumably a vibronic satellite of the B_0 transitions. Isolated 6c-ls heme A^{2+} also exhibits a shoulder ([44]; **Fig. A.3*a*,*b***). However, no vibronic satellite can be seen in the spectrum of heme a^{2+} in C*c*O, except for a tiny band at 420-421 nm (**Fig. 2*c*, 4*f***). The vibronic β-band shows two peaks at ~517 nm and ~560 nm. The one at ~517 nm [11] or both peaks [58] were attributed to heme a^{2+} features. Both peaks are red-

549 shifted by Ca^{2+} and appear in the integral of the Ca^{2+}-induced difference spectrum (**Fig. 2*c***).
550 The first vibrational progression peak, if any, of the a^{2+} B band would therefore be expected at
551 1500 cm^{-1} higher energy than the electronic peak, i.e., at ~419 nm. Therefore, the small 420-
552 nm band in the reconstructed heme a^{2+} spectrum could indeed indicate the presence of a
553 strongly dampened vibronic mode. The reason of the dampening is not yet clear. However,
554 the nearly symmetric lineshape of the heme a^{2+} spectrum is consistent with Soret spectra of
555 other reduced 6c-ls cytochromes, for example, cytochrome c_5 [59–61], neuroglobin [62–66],
556 cytochrome b_{559} [62], superoxide dismutase [62], cytochrome b_{560} [67], cytoglobin [68], and
557 SMR (**Fig. 3*a***). The absence of the shoulder in the spectrum of the 6c-ls heme integrated into
558 the protein could be explained by silencing of the corresponding heme plane vibrations by
559 axial histidines attached to the polypeptide backbone so that out-of-plane movements may be
560 restricted. Heme a_3^{2+} and the free bis-imidazole 6c-ls heme A^{2+} would have this vibrational
561 mode permitted because the heme is either attached to only one histidine or to axial
562 imidazoles that are not connected to any larger scaffold.
563 *4.5. Conclusion and outlook*. Upon reinvestigating the decomposition of the reduced aa_3
564 optical absorption spectrum we propose different contributions of the *a* and a_3 hemes that
565 may resolve long-lasting confusion in the literature. We foresee that this work will be valuable
566 for (re-evaluation of) spectroscopic studies of the C*c*O mechanism. Extension of our approach
567 may come from polarization-sensitive studies in particular on macroscopically ordered
568 systems and true 2-dimensional pump-probe approaches.
569
570 **5. Acknowledgments**
571 Funding: This work was supported by Howard Hughes Medical Institute Award [grant
572 number #55005615] (to AK) and RFBR (Russian Foundation for Basic Research) [grant
573 number #17-04-00160] (to AK). The funding sources had no involvement in study design nor
574 in the collection, analysis and interpretation of data nor in the writing of the report nor in the
575 decision to submit the article for publication.
576
577 **6. Data availability**
578 Numeric data and all scripts used to analyze data and produce figures are downloadable
579 from Mendeley Data: https://data.mendeley.com/datasets/dmrkn9pfrr/3 [69].

580 **Table 1.** Spectral characteristics of hemes a^{2+} and $a_3{}^{2+}$ reported in this work and in previous studies

	Soret band						α-band				source
	overall peak	B_{0y}	B_{0x}	B_{0y}-B_{0x} splitting	B_{0x}/B_{0y} ratio	B_v	overall peak	Q_{0y}	Q_{0x}	Q_{0y}-Q_{0x} splitting	
a^{2+} (bovine)	447.5 (18) 22342 (914)	442 (15) 22609 (741)	451 (15) 22193 (741)	8 416	1.4	420 (18) 23808 (1037)	605 (21) 16517 (567)	593 (17) 16862 (489)	606 (18) 16489 (489)	13 373	This work (Fig.2*c*,4*f*) (Ca^{2+}-shift)
a^{2+} (bovine)	447 (18) 22346 (880)	442.5 (14) 22599 (705)	450 (14) 22218 (705)	7.5 381	1.3	421 (23) 23753 (1295)					This work (Fig.4*f*) (aa_3 photobleaching)
$a_3{}^{2+}$ (bovine)	441 (30) 22664 (1608)	436 (13) 22936 (659)	444 (13.0) 22523 (659)	8 413	2.0	423 (25) 23641(1413)					This work (Fig.4*g*) (aa_3 photobleaching)
$a_3{}^{2+}$ (ba_3)	442.5 (19) 22599 (965)	435 (11) 22972 (589)	444 (12) 22515 (589)	9 457	2.2	427 (15) 23419 (824)					This work (Fig.3*d*) (ba_3 photobleaching)
a^{2+} (bovine)		442-443	450-451	7-9							Fig.1 in [41]
A^{2+} bis-Im in SDS	438 (35) 22831 (1884) extended on blue						593 (39) 16863 (1104)				Fig.6 in [41]
bis-Im A^{2+} ls aqueous buffer	440 (35) 22726 (1841)	436 (22) [a] 22919 (1177)	446 (23) [a] 22428 (1177)	10 [a] 491	1.2 [a]	416 [a] 24033	597 (57) 16750 (1644)				Fig.3B in [44] and Fig. A.3*b* of present paper
bis-Im A^{2+} ls CH_2Cl_2	438 (27) 22830 (1419)	435 (22) [a] 22989 (1177)	442 (23) [a] 22604 (1177)	7 [a] 385	1.0 [a]	414 [a] 24131	592 (41) 16892 (1182)				Fig.4B in [44] and Fig. A.3*d* of present paper
Bis-*n*-butylamine A^{2+} ls Schiff base derivative aqueous buffer	427 (19) 23419 (1023)	425 (16) [a] 23512 (895)	430 (17) [a] 23256 (895)	5 [a] 256	1.0 [a]	407 [a] 24599	573 (29) 17452 (899)				Fig.3B in [44] and Fig. A.3*e*,*f* of present paper
		428 (17) [b] 23374 (922)				409 [b] 24471					
Bis-*n*-butylamine A^{2+} ls Schiff base derivative CH_2Cl_2	428 (18) 23364 (988)	427 (16) [a] 23398 (875)	430 (16) [a] 23256 (875)	3 [a] 142	1.0 [a]	410 [a] 24399	575 (31) 17391 (958)				Fig.4B in [44] and Fig. A.3*g*,*h* of present paper
		429 (16) [b] 23326 (870)				411 [b] 24331					
Bis-1-MeIm A^{2+} ls CH_2Cl_2 (MCD)		430 [c] 23249	442 [c] 22602	12 647				574 [c] 17435	599 [c] 16706	25 729	Fig. 2 in [29]
Bis-1-MeIm A^{2+} ls CH_2Cl_2 (absorption)							588 (32) 17001 (935)				Fig. 7 in [29]
1,2-diMeIm A^{2+} hs CH_2Cl_2 (absorption)							606 (139) 16500 (4493)				Fig. 7 in [29]

581 Format: position (full width at half-height); upper row: nm, lower row: cm^{-1}; [a] 3-gaussian fit in Fig. A.4; [b] 2-gaussian fit in Fig. A.4; [c] positions of the two opposite extrema in

582 the MCD spectrum

References

[1] M. Wikstrom, Proton Pump Coupled to Cytochrome c Oxidase in Mitochondria, Nature. 266 (1977) 271–273.

[2] A.A. Konstantinov, Role of protons in the mechanism of coupling site III of the mitochondrial respiratory chain: cytochrome oxidase as an electronic-protonic generator of membrane potential, Dokl. Akad. Nauk SSSR. 237 (1977) 713–716.

[3] V.Y. Artzatbanov, A.A. Konstantinov, V.P. Skulachev, Involvement of Intramitochondrial Protons in Redox Reactions of Cytochrome a, FEBS Lett. 87 (1978) 180–185.

[4] M. Wikstrom, Cytochrome c oxidase: 25 years of the elusive proton pump, Biochim. Biophys .Acta. 1655 (2004) 241–247.

[5] A.A. Konstantinov, Cytochrome c oxidase: Intermediates of the catalytic cycle and their energy-coupled interconversion, FEBS Lett. 586 (2012) 630–639. https://doi.org/10.1016/j.febslet.2011.08.037.

[6] S.A. Siletsky, A.A. Konstantinov, Cytochrome c oxidase: charge translocation coupled to single-electron partial steps of the catalytic cycle., Biochim. Biophys. Acta. 1817 (2012) 476–88. https://doi.org/10.1016/j.bbabio.2011.08.003.

[7] S. Yoshikawa, K. Muramoto, K. Shinzawa-Itoh, Proton-pumping mechanism of cytochrome C oxidase., Annu. Rev. Biophys. 40 (2011) 205–23. https://doi.org/10.1146/annurev-biophys-042910-155341.

[8] S. Ferguson-Miller, G.T. Babcock, Heme/Copper Terminal Oxidases., Chem. Rev. 96 (1996) 2889–2908. http://www.ncbi.nlm.nih.gov/pubmed/11848844 (accessed September 4, 2013).

[9] S. Yoshikawa, A. Shimada, Reaction mechanism of cytochrome c oxidase., Chem. Rev. 115 (2015) 1936–89. https://doi.org/10.1021/cr500266a.

[10] J.R. Platt, Electronic structure and excitation of polyenes and porphyrins, in: A. Hollaender (Ed.), Radiat. Biol., McGraw-Hill, New York, 1956: pp. 71–123.

[11] W.H. Vanneste, The Stoichiometry and Absorption Spectra of Components a and a3 in Cytochrome c Oxidase, Biochemistry. 65 (1966) 838–848. http://pubs.acs.org/doi/pdf/10.1021/bi00867a005.

[12] M. Wikstrom, K. Krab, M. Saraste, Cytochrome Oxidase - A Synthesis, Academic Press, New York, 1981.

[13] Y. Orii, Determination and Novel Features of the Absolute Absorption Spectra of the Heme a Moieties in Cytochrome c Oxidase, J. Bioenerg. Biomembr. 30 (1998) 47–53.

[14] L.R. Fowler, S.H. Richardson, Y. Hatefi, A rapid method for the preparation of highly purified cytochrome oxidase, Biochim. Biophys. Acta. 64 (1962) 170–173.

[15] T. V Vygodina, A. Kirichenko, A.A. Konstantinov, Cation binding site of cytochrome c oxidase: progress report., Biochim. Biophys. Acta. 1837 (2014) 1188–95. https://doi.org/10.1016/j.bbabio.2014.02.025.

[16] T. Soulimane, U. Gohlke, R. Huber, G. Buse, Three-dimensional crystals of cytochrome-c oxidase from Thermus thermophilus diffracting to 3.8 Å resolution, FEBS Lett. 368 (1995) 132–134. https://doi.org/10.1016/0014-5793(95)00623-H.

[17] O. Farver, Y. Chen, J.A. Fee, I. Pecht, Electron transfer among the Cu A -, heme b - and a 3 - centers of Thermus thermophilus cytochrome ba 3, FEBS Lett. 580 (2006) 3417–3421. https://doi.org/10.1016/j.febslet.2006.05.013.

[18] L. Hederstedt, Cytochrome b reducible by succinate in an isolated succinate dehydrogenase-cytochrome b complex from Bacillus subtilis membranes, J. Bacteriol. 144 (1980) 933–940. https://doi.org/10.1128/jb.144.3.933-940.1980.

[19] G. Cerullo, S. De Silvestri, Ultrafast optical parametric amplifiers, Rev. Sci. Instrum. 74 (2003) 1. https://doi.org/10.1063/1.1523642.

[20] J.J. Snellenburg, S.P. Laptenok, R. Seger, K.M. Mullen, I.H.M. van Stokkum, Glotaran : A Java -Based Graphical User Interface for the R Package TIMP, J. Stat. Softw. 49 (2012) 1–22. https://doi.org/10.18637/jss.v049.i03.
[21] R.H. Byrd, M.E. Hribar, J. Nocedal, An Interior Point Algorithm for Large-Scale Nonlinear Programming, SIAM J. Optim. 9 (1999) 877–900. http://epubs.siam.org/doi/abs/10.1137/S1052623497325107 (accessed December 7, 2015).
[22] R.H. Byrd, J.C. Gilbert, J. Nocedal, A trust region method based on interior point techniques for nonlinear programming, Math. Program. 89 (2000) 149–185. https://doi.org/10.1007/PL00011391.
[23] R.A. Waltz, J.L. Morales, J. Nocedal, D. Orban, An interior algorithm for nonlinear optimization that combines line search and trust region steps, Math. Program. 107 (2006) 391–408. https://doi.org/10.1007/s10107-004-0560-5.
[24] H. Saari, T. Pentilla, M. Wikstrom, Interaction of Ca2+ and H+ with heme A in cytochrome oxidase, J. Bioenerg. Biomembr. 12 (1980) 325–338.
[25] H. Mkrtchyan, T. Vygodina, A.A. Konstantinov, Na+-induced Reversal of the Ca2+-dependent Red Shift of Cytochrome a. Is there a Hydronium Output Well in Cytochrome c Oxidase?, Biochem. Internat. 20 (1990) 183–190.
[26] A. Kirichenko, T. Vygodina, H.M. Mkrtchyan, A. Konstantinov, Specific cation binding site in mammalian cytochrome oxidase., FEBS Lett. 423 (1998) 329–33. http://www.ncbi.nlm.nih.gov/pubmed/9515733 (accessed September 3, 2013).
[27] M. Wikström, H. Saari, A spectral shift in cytochrome a induced by calcium ions., Biochim. Biophys. Acta. 408 (1975) 170–9. http://www.ncbi.nlm.nih.gov/pubmed/811258 (accessed September 3, 2013).
[28] A. V Dyuba, T. V Vygodina, A.A. Konstantinov, Reconstruction of Absolute Absorption Spectrum of Reduced Heme a in Cytochrome c Oxidase from Bovine Heart, (2013).
[29] K. Carter, G. Palmer, Models of the Two Heme Centers in Cytochrome Oxidase, J. Biol. Chem. 257 (1982) 13507–13514. http://www.jbc.org/content/257/22/13507.full.pdf.
[30] J.-L. Martin, M.H. Vos, Femtosecond Biology, Ann. Rev. Biophys. Biomol. Struct. 21 (1992) 199–222.
[31] M.H. Vos, Ultrafast dynamics of ligands within heme proteins, Biochim. Biophys. Acta - Bioenerg. 1777 (2008) 15–31. https://doi.org/10.1016/j.bbabio.2007.10.004.
[32] M.H. Vos, J.L. Martin, Femtosecond processes in proteins, Biochim. Biophys. Acta - Bioenerg. 1411 (1999) 1–20. https://doi.org/10.1016/S0005-2728(99)00035-3.
[33] M.H. Vos, V.B. Borisov, U. Liebl, J.L. Martin, A.A. Konstantinov, Femtosecond resolution of ligand-heme interactions in the high-affinity quinol oxidase bd: A di-heme active site?, Proc. Natl. Acad. Sci. U. S. A. 97 (2000) 1554–1559. https://doi.org/10.1073/pnas.030528197.
[34] C. Hägerhäll, C. Von Wachenfeldt, L. Hederstedt, R. Aasa, Two Hemes in Bacillus subtilis Succinate : Menaquinone Oxidoreductase (Complex II), Biochemistry. 31 (1992) 7411–7421. https://doi.org/10.1021/bi00147a028.
[35] I. V. Shelaev, F.E. Gostev, T. V. Vygodina, S. V. Lepeshkevich, B.M. Dzhagarov, Femtosecond absorption spectroscopy of cytochrome c oxidase: Excited electronic states and relaxation processes in heme a and heme a3 centers, High Energy Chem. 52 (2018) 45–51. https://doi.org/10.1134/S0018143918010101.
[36] I. V. Shelaev, F.E. Gostev, T. V. Vygodina, S. V. Lepeshkevich, B.M. Dzhagarov, Femtosecond Absorption Spectroscopy of Reduced and Oxidized Forms of Cytochrome c Oxidase: Excited States and Relaxation Processes in Heme a and a3 Centers, Opt. Spectrosc. 127 (2019) 756–762. https://doi.org/10.1134/S0030400X19100278.
[37] G.L. Liao, G. Palmer, The reduced minus oxidized difference spectra of cytochromes a and a3, Biochim. Biophys. Acta - Bioenerg. 1274 (1996) 109–111. https://doi.org/10.1016/0005-

2728(96)00014-X.
[38] J.W. Petrich, C. Poyart, J.L. Martin, Photophysics and Reactivity of Heme Proteins: A Femtosecond Absorption Study of Hemoglobin, Myoglobin, and Protoheme, Biochemistry. 27 (1988) 4049–4060. https://doi.org/10.1021/bi00411a022.
[39] P. Stoutland, J.-C. Lambry, J.-L. Martin, W.H. Woodruff, Femtosecond Dynamics of reduced Cytochrome Oxidase and its CO derivative, J. Phys. Chem. 95 (1991) 6406–6408.
[40] U. Liebl, G. Lipowski, M. Négrerie, J.-C. Lambry, J.-L. Martin, M.H. Vos, Coherent reaction dynamics in a bacterial cytochrome c oxidase, Nature. 401 (1999) 181–184. https://doi.org/10.1038/43699.
[41] J.S. Felsch, M.P. Horvath, S. Gursky, M.R. Hobaugh, P.N. Goudreau, J.A. Fee, W.T. Morgan, S.J. Admiraal, M. Ikeda-Saito, T. Fujiwara, Y. Fukumori, T. Yamanaka, R.A. Copeland, Probing protein-cofactor interactions in the terminal oxidases by second derivative spectroscopy: Study of bacterial enzymes with cofactor substitutions and heme a model compounds, Protein Sci. 3 (1994) 2097–2103. https://doi.org/10.1002/pro.5560031123.
[42] D. Sherman, S. Kotake, N. Ishibe, R.A. Copeland, Resolution of the Electronic Transitions of Cytochrome c Oxidase: Evidence for Two Conformational States of Ferrous Cytochrome a, Proc. Natl. Acad. Sci. USA. 88 (1991) 4265–4269.
[43] D. Wilson, M. Gilmour, The low-temperature spectral properties of mammalian cytochrome oxidase. I. The enzyme in intact rat-liver mitochondria, Biochim. Biophys. Acta - Bioenerg. (1967). http://www.sciencedirect.com.sci-hub.io/science/article/pii/0005272867901089 (accessed December 17, 2015).
[44] S.W. Han, Y.C. Ching, S.L. Hammes, D.L. Rousseau, Vibrational structure of the formyl group on heme a. Implications on the properties of cytochrome c oxidase, Biophys. J. 60 (1991) 45–52. https://doi.org/10.1016/S0006-3495(91)82029-X.
[45] K. Kopcova, L. Blascakova, T. Kozar, D. Jancura, M. Fabian, Response of Heme Symmetry to the Redox State of Bovine Cytochrome c Oxidase, Biochemistry. 57 (2018) 4105–4113. https://doi.org/10.1021/acs.biochem.8b00459.
[46] M.K. Wikstrom, H.J. Harmon, W.J. Ingledew, B. Chance, A Re-evaluation of the Spectral, Potentiometric, and Energy-Linked Properties of Cytochrome c Oxidase in Mitochondria, FEBS Lett. 65 (1976) 259–277.
[47] M.C. Rocha, R. Springett, Spectral components of detergent-solubilized bovine cytochrome oxidase, Biochim. Biophys. Acta - Bioenerg. 1859 (2018) 555–566. https://doi.org/10.1016/j.bbabio.2018.04.009.
[48] E.S. Manas, J.M. Vanderkooi, K.A. Sharp, The Effects of Protein Environment on the Low Temperature Electronic Spectroscopy of Cytochrome c and Microperoxidase-11, J. Phys. Chem. B. 103 (1999) 6334–6348. https://doi.org/10.1021/jp9908552.
[49] K.S. Reddy, P.J. Angiolillo, W.W. Wright, M. Laberge, J.M. Vanderkooi, Spectral splitting in the α (Q0.0) absorption band of ferrous cytochrome c and other heme proteins, Biochemistry. 35 (1996) 12820–12830. https://doi.org/10.1021/bi960895l.
[50] V. Sanfratello, A. Boffi, A. Cupane, M. Leone, Heme symmetry, vibronic structure, and dynamics in heme proteins: Ferrous nicotinate horse myoglobin and soybean leghemoglobin, Biopolym. - Biospectroscopy Sect. 57 (2000) 291–305. https://doi.org/10.1002/1097-0282(2000)57:5<291::AID-BIP60>3.0.CO;2-O.
[51] M. Levantino, Q. Huang, A. Cupane, M. Laberge, A. Hagarman, R. Schweitzer-Stenner, The importance of vibronic perturbations in ferrocytochrome c spectra: A reevaluation of spectral properties based on low-temperature optical absorption, resonance Raman, and molecular-dynamics simulations, J. Chem. Phys. 123 (2005) 054508. https://doi.org/10.1063/1.1961556.
[52] J.A. Cowan, H.B. Gray, Q-Band Splitting in the Spectra of Heme Proteins, Inorg. Chem. 28 (1989) 4554–4556. https://doi.org/10.1021/ic00324a026.

[53] W.B. Elliott, E. Margoliash, High Resolution Low Temperature Spectrophotometry of Cytochromes c, in: Dev. Appl. Spectrosc., Springer US, 1971: pp. 125–140. https://doi.org/10.1007/978-1-4757-0782-3_5.
[54] J.A. Shelnutt, The Raman excitation spectra and absorption spectrum of a metalloporphyrin in an environment of low symmetry, J. Chem. Phys. 72 (1980) 3948. https://doi.org/10.1063/1.439664.
[55] G.T. Babcock, P.M. Callahan, Redox-Linked Hydrogen Bond Strength Changes in Cytochrome a: Implications for a Cytochrome Oxidase Proton Pump, Biochemistry. 22 (1983) 2314–2319.
[56] S. Riistama, M.I. Verkhovsky, L. Laakkonen, M. Wikström, A. Puustinen, Interaction between the formyl group of heme a and arginine 54 in cytochrome aa(3) from Paracoccus denitrificans., Biochim. Biophys. Acta. 1456 (2000) 1–4. http://www.ncbi.nlm.nih.gov/pubmed/10611451 (accessed September 5, 2013).
[57] H. Lee, T.K. Das, D.L. Rousseau, D. Mills, S. Ferguson-Miller, R.B. Gennis, Mutations in the Putative H-Channel in the Cytochrome c Oxidase from Rhodobacter sphaeroides Show That This Channel Is Not Important for Proton Conduction but Reveal Modulation of the Properties of Heme a †, Biochemistry. 39 (2000) 2989–2996. https://doi.org/10.1021/bi9924821.
[58] A. V Dyuba, T. Vygodina, N. Azarkina, A.A. Konstantinov, Calcium ions inhibit reduction of heme a in bovine cytochrome c oxidase., FEBS Lett. 589 (2015) 3853–8. https://doi.org/10.1016/j.febslet.2015.11.023.
[59] A.I. Cederbaum, Molecular mechanisms of the microsomal mixed function oxidases and biological and pathological implications, Redox Biol. 4 (2015) 60–73. https://doi.org/10.1016/j.redox.2014.11.008.
[60] Y. Yoshida, Y. Tamura-Higashimaki, R. Sato, Purification and characterization of intact cytochrome b5 from yeast microsomes, Arch. Biochem. Biophys. 220 (1983) 467–476. https://doi.org/10.1016/0003-9861(83)90437-X.
[61] P.L. Holmans, M.S. Shet, C.A. Martin-Wixtrom, C.W. Fisher, R.W. Estabrook, The High-Level Expression in Escherichia coli of the Membrane-Bound Form of Human and Rat Cytochrome b5 and Studies on Their Mechanism of Function, Arch. Biochem. Biophys. 312 (1994) 554–565.
[62] M.H. Vos, A. Battistoni, C. Lechauve, M.C. Marden, L. Kiger, A. Desbois, E. Pilet, E. de Rosni, U. Liebl, Ultrafast heme-residue bond formation in six-coordinate heme proteins: implications for functional ligand exchange, Biochem. 47 (2008) 5718–5723.
[63] J.T. Trent III, M.S. Hargrove, A ubiquitously expressed human hexacoordinate hemoglobin, J. Biol. Chem. 277 (2002) 19538–19545.
[64] L. Li, H. Ji, C. Zhao, T. Xu, G. Liu, C. Fu, H. Yan, Expression, purification and spectra characterization of neuroglobin, Chinese Sci. Bull. 50 (2005) 1708–1713. https://doi.org/10.1360/982004-618.
[65] A. Giuffrè, T. Moschetti, B. Vallone, M. Brunori, Neuroglobin: Enzymatic reduction and oxygen affinity, Biochem. Biophys. Res. Commun. 367 (2008) 893–898. https://doi.org/10.1016/j.bbrc.2008.01.021.
[66] K. Nienhaus, G.U. Nienhaus, Probing heme protein-ligand interactions by UV/visible absorption spectroscopy., Methods Mol. Biol. 305 (2005) 215–242. https://doi.org/10.1385/1-59259-912-5:215.
[67] L. Yu, J.X. Xu, P.E. Haley, C.A. Yu, Properties of bovine heart mitochondrial cytochrome b560, J. Biol. Chem. 262 (1987) 1137–1143. https://doi.org/10.1016/s0021-9258(19)75761-5.
[68] P. Beckerson, M.T. Wilson, D.A. Svistunenko, B.J. Reeder, Cytoglobin ligand binding regulated by changing haem-co-ordination in response to intramolecular disulfide bond formation and lipid interaction, Biochem. J. 465 (2015) 127–137.

https://doi.org/10.1042/BJ20140827.
[69] A. Diuba, Data and scripts for “Individual heme a and heme a3 contributions to the Soret absorption spectrum of the reduced bovine cytochrome c oxidase,” 2 (2022). https://doi.org/10.17632/DMRKN9PFRR.3.